NeuroImage 322 (2025) 121553

Contents lists available at ScienceDirect

NeuroImage

journal homepage: www.elsevier.com/locate/ynimg

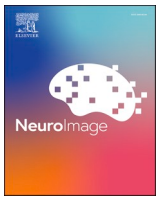

Predictive modeling of TMS-evoked responses: Unraveling instantaneous excitability states

Oskari Ahola [a,b,d], Lisa Haxel [a,b,c], Maria Ermolova [a,b], Dania Humaidan [a,b], Tuomas P. Mutanen [d], Mikael Laine [d], Matilda Makkonen [d], Elena Ukharova [d,e], Timo Roine [d], Pantelis Lioumis [d,e], Roberto Guidotti [f,g], Risto J. Ilmoniemi [d], Ulf Ziemann [a,b,*]

[a] Hertie Institute for Clinical Brain Research, University of Tubingen, Tubingen, Germany
[b] Department of Neurology and Stroke, University of Tübingen, Tübingen, Germany
[c] Excellence Cluster Machine Learning, University of Tübingen, Tübingen, Germany
[d] Department of Neuroscience and Biomedical Engineering, Aalto University, Espoo, Finland
[e] BioMag Laboratory, HUS Medical Imaging Center, Aalto University, University of Helsinki and Helsinki University Hospital, Helsinki, Finland
[f] Institute for Advanced Biomedical Technologies, University of Chieti-Pescara, Chieti, Italy
[g] Department of Neuroscience and Imaging, University of Chieti-Pescara, Chieti, Italy

ARTICLE INFO

Keywords:
Cortical excitability
Corticospinal excitability
TMS
EEG
TMS-evoked potential
Motor evoked potential
Single-trial TEP

ABSTRACT

Transcranial magnetic stimulation (TMS) combined with electroencephalography (EEG) and electromyography (EMG) provides a unique window into instantaneous cortical and corticospinal excitability states. We investigated 50 healthy participants to determine how fluctuations in pre-stimulus brain activity influence single-trial TMS-evoked potentials (TEPs) and motor-evoked potentials (MEPs). We developed a novel automated source-level TEP extraction method using individualized spatiotemporal priors that is robust against poor single-trial signal-to-noise ratios (SNRs) and ongoing oscillations. TEP and MEP amplitudes were predicted with linear mixed-effects models based on pre-stimulation EEG band-powers (theta to gamma), while accounting for temporal drifts (within-session trends), coil control, and inter-subject differences. We found that higher pre-stimulus sensorimotor alpha, beta, and gamma power were each associated with larger TEPs, indicating a more excitable cortical state. Increases in alpha and gamma power immediately before stimulation specifically predicted larger MEPs, reflecting increased corticospinal excitability. These results reveal relationships between ongoing oscillatory brain states and TMS response amplitudes, identifying EEG biomarkers of high- and low-excitability states. In conclusion, our study demonstrates the feasibility of single-trial source-level TMS–EEG analysis and shows that spontaneous alpha-, beta-, and gamma-band oscillations modulate motor cortical and corticospinal responsiveness. These findings can contribute to EEG-informed, brain-state-dependent TMS protocols in optimizing neuromodulatory interventions in clinical and research applications.

1. Introduction

Combining transcranial magnetic stimulation (TMS) with electroencephalography (EEG) and electromyography (EMG) provides instantaneous information about cortical and corticospinal excitability states via TMS-related responses, such as TMS-evoked potentials (TEPs) and motor-evoked potentials (MEPs) (Ilmoniemi et al., 1997; Ilmoniemi and Kičić 2010; Hallett 2007). These neurophysiological measures reflect the responsiveness and plasticity of targeted cortical regions (Pellicciari et al. 2018; Gosseries et al. 2015; Voineskos et al. 2019) and are predictive markers of outcome in neurological and psychiatric disorders, including stroke and depression (Lefaucheur et al. 2020; Vucic et al. 2023; Strafella et al. 2023; Bembenek et al. 2020; Hordacre et al. 2019). Indeed, patients with a variety of brain network disorders who exhibit larger TMS-evoked responses often respond better to therapeutic interventions (Pellicciari et al. 2018; Bembenek et al. 2020; Strafella et al. 2023).

Despite their clinical relevance, TMS-evoked responses show

* Corresponding author.
E-mail address: ulf.ziemann@uni-tuebingen.de (U. Ziemann).

https://doi.org/10.1016/j.neuroimage.2025.121553
Received 18 June 2025; Received in revised form 18 September 2025; Accepted 21 October 2025
Available online 30 October 2025

substantial variability within and across individuals (Lioumis et al. 2009). This variability is partly driven by changing neuronal activity states (Voineskos et al. 2019) – as well as differences in structural connectivity (Casarotto et al. 2010). However, the specific electrophysiological features that determine whether the brain is in a high- or low-excitability state remain poorly understood. In particular, it is unclear how inhibitory and excitatory network dynamics before TMS influence the resulting TEP and MEP amplitudes. As a result, current standard TMS protocols ignore the momentary brain state and may deliver stimuli at suboptimal times, potentially compromising therapeutic success.

Recent evidence has begun to investigate how pre-stimulus EEG rhythms modulate TMS outcomes. Alpha-frequency oscillations were traditionally thought to index cortical inhibition, with higher alpha power suppressing excitability (Klimesch et al. 2007). Contrary to this notion, real-time EEG-triggered TMS studies have demonstrated pulsed facilitation of corticospinal excitability at specific phases of the sensorimotor μ-alpha-cycle, even finding that high alpha power can coincide with larger rather than smaller MEPs (Bergmann et al. 2019; Zrenner et al. 2018). Similarly, beta-frequency oscillations in motor cortex have been linked to the maintenance of the current sensorimotor state and GABAergic inhibitory tone, yet their exact relationship to excitability is complex (Groth et al. 2021). Gamma-band activity, reflecting local cortical excitatory–inhibitory circuit engagement, may conversely signal periods of heightened neuronal firing and readiness (Herrmann et al. 2010). Overall, these studies suggest that instantaneous oscillatory activity in multiple frequency bands could serve as a proxy for the brain's excitability state, but a comprehensive, multi-band characterization of this relationship at the single-trial level is lacking. Furthermore, prior TMS–EEG studies often focused on sensor-level EEG or averaged responses, leaving open the question of how to reliably quantify single-trial TEPs from cortical sources.

To address these gaps, we present a methodology for single-trial source-level TEP analysis that accounts for the low spatiotemporal signal-to-noise ratio (SNR) of individual TMS–EEG trials. In the present study, we leverage this approach to explore the relationship between pre-stimulation EEG dynamics and subsequent TMS-evoked responses in a sample of 50 healthy adults. Specifically, we examine whether oscillatory power in canonical frequency bands prior to stimulation can predict the amplitude of the induced TEPs in the targeted cortex and the corresponding MEPs in the periphery. By identifying robust EEG markers of instantaneous cortical and corticospinal excitability, our work aims to deepen the neurophysiological understanding of TMS response variability. Importantly, these insights also lay groundwork for brain-state-dependent TMS protocols, whereby stimulation can be timed to an optimal excitability state to enhance neuromodulatory effects. Such EEG-informed TMS strategies hold promise for increasing the efficacy of therapeutic and rehabilitative interventions across a range of brain disorders.

2. Methods

We conducted a study investigating TMS-evoked EEG and motor responses at two European research centers in the ConnectToBrain synergy project funded by the European Research Council (grant no 810377). The experimental protocol was standardized while accommodating for site-specific equipment variation.

2.1. Data acquisition

The measurements were performed by two research groups: the Brain Networks & Plasticity Laboratory at the Hertie Institute for Clinical Brain Research, University of Tübingen, Germany, and the TMS Group at the Department of Neuroscience and Biomedical Engineering, Aalto University, Finland.

The combined dataset consists of 50 healthy right-handed participants (28 women) of ages 28 $\pm$ 6 years (mean $\pm$ standard deviation). The TMS–EEG measurement contained four blocks of 300 biphasic single pulses at an intensity of 110 % of the resting motor threshold (rMT) targeted at the left motor hotspot with a randomized inter-trial interval of 4.0–4.5 or 2.5–3.5 s, in Aalto and Tübingen, respectively. RMT was defined as the minimum stimulation intensity that resulted in MEPs with a minimum peak-to-peak difference of 50 μV in at least 50% of trials (Rossini et al. 2015).

The TMS–EEG data were recorded with TMS-compatible NeurOne 128- and 64-channel EEG systems (Bittium Ltd, Finland) with a sampling rate of 5 kHz. EMG was recorded from the right abductor pollicis brevis (APB) and the first dorsal interosseus (FDI) muscles in a bipolar belly–tendon montage. In NeurOne, the data were causally lowpass filtered (tap lengths of 3.4 and 9 ms in Aalto and Tübingen, respectively) from 1250 Hz. TMS was administered with a Nexstim NBS 5.2.4 or NBT 2.2.4 (Nexstim Plc, Finland) system with a Nexstim cooled coil (Aalto) or with a MagVenture (MagVenture A/S, Denmark) R30 or X100 stimulator with a Cool-B65 coil (Tübingen). Neuronavigation was performed using individual T1-weighted magnetic resonance images (MRIs) with Nexstim or Localite (Localite GmbH, Germany) systems in Aalto and Tübingen, respectively. The TMS click sound was masked with individually calibrated noise (Russo et al. 2022) using ER-3C insert earphones (Etymotic Research Ltd, United States).

T1- and T2-weighted MRIs were acquired with magnetization-prepared rapid acquisition gradient echo (MPRAGE) and turbo spin echo (TSE) sequences, respectively, using 3T Siemens Skyra and Prisma scanners (Siemens Plc, Germany). For further specification on experimental details, see Section 1 in the Supplementary Materials.

All subjects gave their written informed consent for participating in the study, which was approved by the ethics committees of the University of Tübingen (810/2021BO2) and the Helsinki University Hospital (HUS/1198/2016). The study was conducted in compliance with the Declaration of Helsinki.

2.2. Preprocessing

The TMS–EEG data were preprocessed with Matlab 2024a (The MathWorks Inc, United States) using custom scripts and EEGLAB 2024.2 (Delorme and Makeig 2004) with the TESA toolbox (Rogasch et al. 2017; Mutanen et al. 2020) in an automated fashion. The pre- and post-stimulus periods, which were initially defined to be $[-1250, -25)$ and $[-20, 300)$ ms relative to the TMS pulse, respectively, were processed separately to not violate direct pre–post causality.

We interpolated TMS pulse artifacts and removed noisy channels by separately considering both periods. We then calibrated independent component analysis (ICA) (Hyvärinen and Oja 2000; Pion-Tonachini et al. 2019) filters using pooled pre-stimulus data that had been highpass filtered at 2 Hz, compressed to 35 dimensions using principal component analysis (PCA), and average referenced, in order to suppress ocular artifacts. The calibrated filters were subsequently applied to non-filtered and non-PCA-compressed average-referenced pre- and post-stimulus periods. This way of applying ICA also mitigates suppressing TEP-related neuronal activity that could be mixed in the ICA filters if the ICA decomposition was derived from both pre- and post-stimulus periods.

For the pre-stimulus period, we reconstructed bad channels via spherical spline interpolation, applied 4th-order zero-phase Butterworth bandpass and powerline bandstop filtering ($2-$ $-$ 90, and $48-$ $-$ 52 Hz, respectively), downsampled the data to 1000 Hz, and cropped the data to $[-1045, -45)$ ms. We then rejected trials based on standardized standard deviation statistics of the pre-stimulus period.

For the pooled post-stimulus-focused periods, we suppressed noise and reconstructed contaminated channels using the source-estimate-utilizing noise-discarding (SOUND) algorithm (Mutanen et al. 2018). We then suppressed muscle artifacts with the signal-space-projection-source-informed reconstruction (SSP–SIR)

algorithm (Mutanen et al. 2016), and re-interpolated an extended TMS pulse artifact window. After cropping the post-stimulus period to [–20, 150] ms, we removed bad trials based on standardized standard deviation statistics of the post-stimulus period. The post-stimulus baseline correction range was [–20, –10] ms. The pre- and post-stimulus data were analyzed in average reference. Contrary to common practices, we do not downsample or directly bandpass filter our post-stimulus data to avoid additional temporal smearing and edge effects.

EMG preprocessing included baseline correction, linear detrending, and pre-innervation-based trial exclusion within the pre-stimulation window of [–100, –10] ms. We extracted MEP amplitudes as the peak-to-peak (*i.e.*, minimum-to-maximum voltage difference) from [20,50] ms of each trial from the channel with the average higher amplitude. Detailed preprocessing specifications on channel and trial rejection, hyperparameters, baseline corrections, and intermediate referencing and time range selections, are provided in Section 2 in the Supplementary Materials.

2.3. TEP extraction

Equivalent current dipoles can be used to represent small source-current concentrations (Henderson et al. 1975; Sarvas 1987). The TMS-evoked potentials (TEPs) for each trial were modeled by the amplitude of time-constrained, fixed-position, fixed-orientation current dipole fits. When fitting dipoles to single-trial data, we used prior temporal, spatial, and orientational information from the average response to mitigate the effect of poor single-trial SNR and ongoing oscillations that are prevalent in sensor-level data. The best-fitting dipoles in the average response were automatically identified using pseudoinverse by maximizing the coefficient of determination (R^2) and response stability.

For each response, we initially defined the following time ranges **T**: N15: [12,25], P30: [25,40], N45: [40,55], and P60: [55,73] ms. Fitting was done in reverse temporal order. To avoid response overlapping, the upper edge of each time window prior to P60 was sequentially adjusted to ensure a minimum 5-ms gap from the minimum time of the subsequent response.

For each response, we defined candidate dipoles $\widehat{\mathbf{Q}}_t$ at positions $\widehat{\mathbf{r}}_t$ for each time point $t \in \mathbf{T}$ as

$$\{\widehat{\mathbf{Q}}_t, \widehat{\mathbf{r}}_t\} = \underset{\mathbf{r},\ \mathbf{Q}}{\operatorname{argmax}}\ R^2(\overline{\mathbf{m}}(t), \mathbf{L}(\mathbf{r})\mathbf{Q}),$$

where **Q** is the dipole moment, $\overline{\mathbf{m}}$ is trial-averaged EEG data **m**, t is the time, and $\mathbf{L}(\mathbf{r})$ is the lead field at position **r**.

For each dipole $\widehat{\mathbf{Q}}_t$ at $\widehat{\mathbf{r}}_t$, we defined activation time ranges $\widehat{\mathbf{T}}_t \subseteq \mathbf{T}$ around t as continuous intervals during which the dipole fixed at $\widehat{\mathbf{r}}_t$ had at least 90% of the R^2 and deviated no >10 degrees relative to $\widehat{\mathbf{Q}}_t$ with an unit-length orientation $\widehat{\mathbf{q}}_t$. To prioritize long intervals while mitigating the effect of prolonged low-amplitude dipolar (resulting in sufficient R^2) activity with little spatial variability, the optimal fitting time range $\widehat{\mathbf{T}}$ for the response was then defined as the interval,

$$\widehat{\mathbf{T}} = \underset{\widehat{\mathbf{T}}_t \subseteq \mathbf{T}}{\operatorname{argmax}}\ |\widehat{\mathbf{T}}_t| \overline{R}^2_{\widehat{\mathbf{T}}_t} \sqrt{\overline{A}_{\widehat{\mathbf{T}}_t}},$$

where $\overline{A}_{\widehat{\mathbf{T}}_t}$ (in units of nAm) and $\overline{R}^2_{\widehat{\mathbf{T}}_t}$ are the average dipole amplitude and R^2, respectively, in time range $\widehat{\mathbf{T}}_t$. The optimal dipole position $\widehat{\mathbf{r}}$ and orientation $\widehat{\mathbf{q}}$ correspond to this time window.

Finally, for each trial i, the dipole fixed at $\widehat{\mathbf{r}}$ with orientation $\widehat{\mathbf{q}}$ in time range $\widehat{\mathbf{T}}$ was selected as

$$\widehat{\mathbf{Q}}_i = \underset{t \in \widehat{\mathbf{T}}}{\operatorname{argmax}}\ R^2(\mathbf{m}_i(t), \mathbf{L}(\widehat{\mathbf{r}})a(t)\widehat{\mathbf{q}}),$$

The scalar amplitude $a(t)$ — obtained by solving $\mathbf{m}_i(t) = a(t)\mathbf{L}(\widehat{\mathbf{r}})\widehat{\mathbf{q}}$ using least squares — of a best-fitting fixed-orientation dipole $\mathbf{Q} = a\widehat{\mathbf{q}}$, can be negative due to polarity reversal. We use the absolute amplitude to represent the magnitude of cortical excitation. To mitigate artifactual effects and to address poor single-trial SNR, for each response, we only included subjects whose optimal dipole fit to the average response (resulting in time range $\widehat{\mathbf{T}}$) had an R^2 of at least 75% and an amplitude of at least 20 nAm. The extraction procedure is illustrated in Fig. 1.

2.4. Feature extraction

We performed source-space analysis using subject-specific MRIs for the pre-stimulation period [–1045, –45 ms] using MNE Python 1.7.0 (Gramfort et al. 2013) and custom scripts. Source estimates were acquired with minimum-norm estimation (MNE) (Hämäläinen and Ilmoniemi 1994), projected onto the *fsaverage* brain, and parcellated according to the Desikan–Killiany atlas (Desikan et al. 2006). To investigate effects near response and stimulation locations, source-space signals were also extracted from custom parcels defined as source-point clusters with maximal geodesic distances of 2 cm to the nearest source positions of a) the individual response (dipole) locations and b) the MNI-Talairach left motor hand knob at (–40, –20,62) mm.

For each parcellated pre-stimulus time series, we calculated power spectral densities (PSDs) for the theta, alpha, beta, and gamma frequency bands with the multi-taper method. The frequency bands were determined individually based on individual peak alpha-power frequency (Klimesch 1999), identified from the average pre-stimulus sensor space PSD. This resulted in average frequency ranges of theta = 3.8–7.3, alpha = 7.3–12.3, beta = 12.3–32.3, and gamma = 32.3–82.3 Hz.

For each trial, the coil control (stimulation accuracy) value was computed as a weighted average of the differences between the actual and target stimulation parameters — specifically position (in units of mm), normal, and direction (in degrees). To emphasize deviations in coil position (which tend to be more variable than orientation) and to reduce possible multicollinearity, we applied weights of 0.7 for position and 0.15 for normal and direction. Missing coil control data (6.2% of trials) was handled with median replacement. Further information on feature extraction is available in Section 4 in the Supplementary Materials.

2.5. Predictive modeling

We predicted log-transformed absolute dipole (source-localized TEP) and MEP amplitudes using linear mixed-effect models (LMMs) (Lindstrom and Bates 1988; Seabold and Perktold 2010) with subject-level random effects as

$$\mathbf{A}_{\text{response},k} \sim \mathbf{P}_k + \mathbf{c} + \boldsymbol{\tau} + \mathbf{P}_k * \boldsymbol{\tau} + (1|\text{Subject}),$$

where $\mathbf{P}_k$ are the band-powers of each frequency band (theta, alpha, beta, and gamma) in parcel (brain region) k and **c** is the coil control for each trial (weighted pose deviances from the target). $\boldsymbol{\tau}$ is the maximum-normalized post-processed trial number for each subject (proxy for time, referred as such from here onwards), and $\mathbf{P}_k * \boldsymbol{\tau}$ denotes the interaction between band-power and time.

We log-transformed power, time, and coil control parameters and standardized them zero-mean and unit variance. Powers were within-subject standardized to account for subject-specific baselines and variability, and the time and coil control were globally standardized. While our primary focus is the effect of fluctuations in power, we included the coil control as a covariate to account for targeting accuracy — a known confound in TMS. Additionally, we included band-power–time interactions to distinguish instantaneous fluctuations from over-time trends that may exist between power-based predictors and response amplitudes.

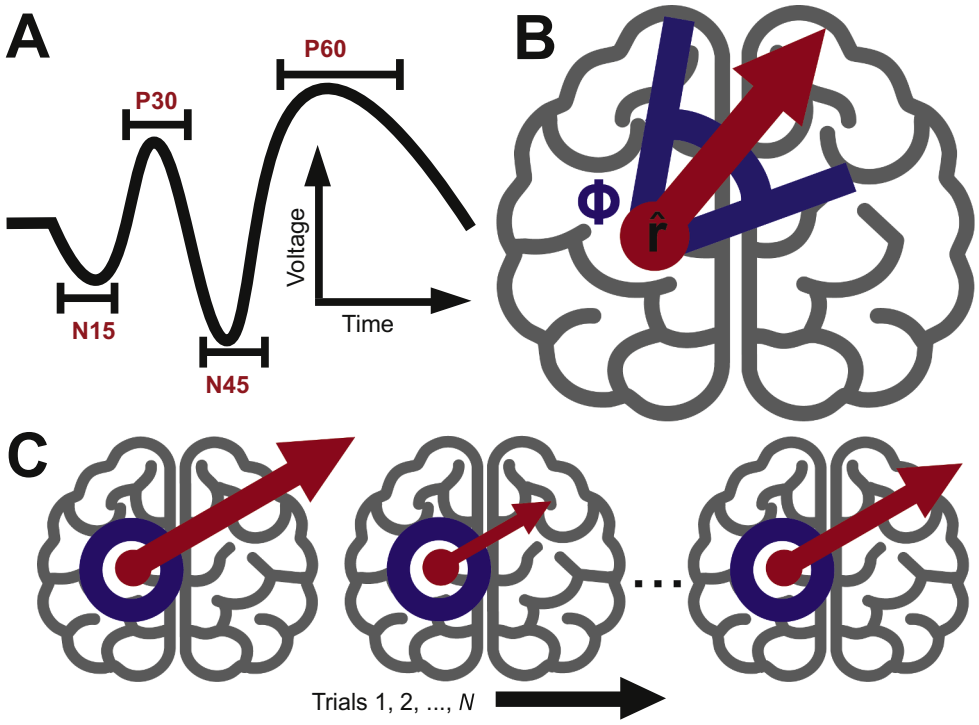

Fig. 1. TEP extraction procedure. **A**: Illustration of TEP components with fitting time ranges determined by maximizing dipole coefficient of determination (R^2), amplitude, and orientation stability. The fitting range was adjusted to ensure a minimum 5-ms gap to the subsequent response. **B**: Determination of an extraction time range $\hat{\boldsymbol{T}}$ for a response where dipole orientations fitted to the dipole position $\hat{\boldsymbol{r}}$ deviated less than $\phi = 10$ degrees and had an R^2 of at least 90% relative to the optimal dipole. **C**: Fixed-orientation dipoles with different amplitudes modeling single-trial responses fitted to fixed positions $\hat{\boldsymbol{r}}$. The figure was created with Adobe Illustrator using the Text to Vector graphics tool for the brains.

2.6. Statistics

The two-tailed p-values of the LMM coefficients were determined using Wald t-tests. The p-values were corrected for multiple comparisons with the Bonferroni method while excluding the model intercept (Seabold and Perktold 2010). All p-values of LMM coefficients reported in this text have been Bonferroni-corrected. LMM goodness-of-fits were evaluated using conditional and marginal R^2 (Nakagawa and Schielzeth 2013); see Section 5.2 in the Supplementary Materials.

The two-tailed p-values of Spearman correlation coefficients were computed using the t-distribution under the null hypothesis of no monotonic relationship (Virtanen et al. 2020).

3. Results

3.1. Predictive features

We found several predictors of TEP and MEP amplitude across multiple parcels (brain regions). The strongest positive TEP predictors were at the alpha, beta, and gamma bands and spatially similar across especially temporally adjacent responses. TEPs with longer latencies (N45 and P60) were more positively affected by changes in bilateral centro-parietal beta and bilateral sensorimotor gamma power, whereas the earlier TEPs (N15 and P30) were more affected by bilateral sensorimotor or parietal alpha power. P30 was also positively modulated by frontal beta power.

MEPs were most positively affected by ipsilateral (on the side of stimulation) sensorimotor alpha-frequency (similar to the sensorimotor μ-rhythm) and bilateral frontal gamma power. These findings align with previous research (Thies et al. 2018; Wischnewski et al. 2022; Haxel et al. 2025).

We compared the absolute feature-specific coefficients across the models from the custom and anatomical parcels (see Section 2.4) to determine which features in specific regions exert greater influence on response amplitudes. At the custom motor hand-knob parcel, the predictive alpha power coefficient for MEPs was the at the 100th percentile ($\beta = 0.07$) and at the 97th percentile for N15 ($\beta = 0.04$), and the gamma power coefficient of P60 was at the 97th percentile ($\beta = 0.04$). Gamma power yielded similar effects at the response-location derived parcels for N15, P30, and N45 ($\beta = 0.03$; 100th, 97th, and 98th percentiles, respectively), and P60 ($\beta = 0.04$; 100th percentile). Similarly, the beta power coefficient at the response-location derived parcel was at the 97th percentile for N45 ($\beta = 0.02$) and at the 98th percentile for P60 ($\beta = 0.03$). The band-power coefficients for each response on each anatomical label are displayed in Fig. 2.

The ongoing measurement time (*i.e.*, trends; modeled with trial numbers) was a positive predictor for MEPs, with a maximum coefficient strength of $\beta = 0.11$ ($p < 0.05$). The effect was not notable for TEPs with a maximum of $\beta = 0.02$ ($p < 0.05$) for N15. The band-power–time interaction terms yielded smaller coefficients: $|\beta| < 0.03$ for TEPs and $|\beta| < 0.04$ for MEPs (both $p < 0.05$). Most notably, MEP was negatively modulated by gamma power trends and positively by alpha power trends. Visualization is provided in Section 5.1 in the Supplementary Materials.

The coil deviations (subject means; position: 2.2 ± 1.0 mm, direction: 1.3 ± 0.7, and normal: 1.3 ± 0.8 degrees) had small effects on N15 (minimum of $\beta = -0.04$) and larger maximal negative effect on MEPs ($\beta = -0.14$); both $p < 0.05$.

3.2. Response stability and correlations

Stability across different outcome measures provide essential information on inter-response relationships, and consequently, differences between cortical and corticospinal excitability. Assessing these factors increases overall fidelity of the modeled low SNR single-trial TMS–EEG responses.

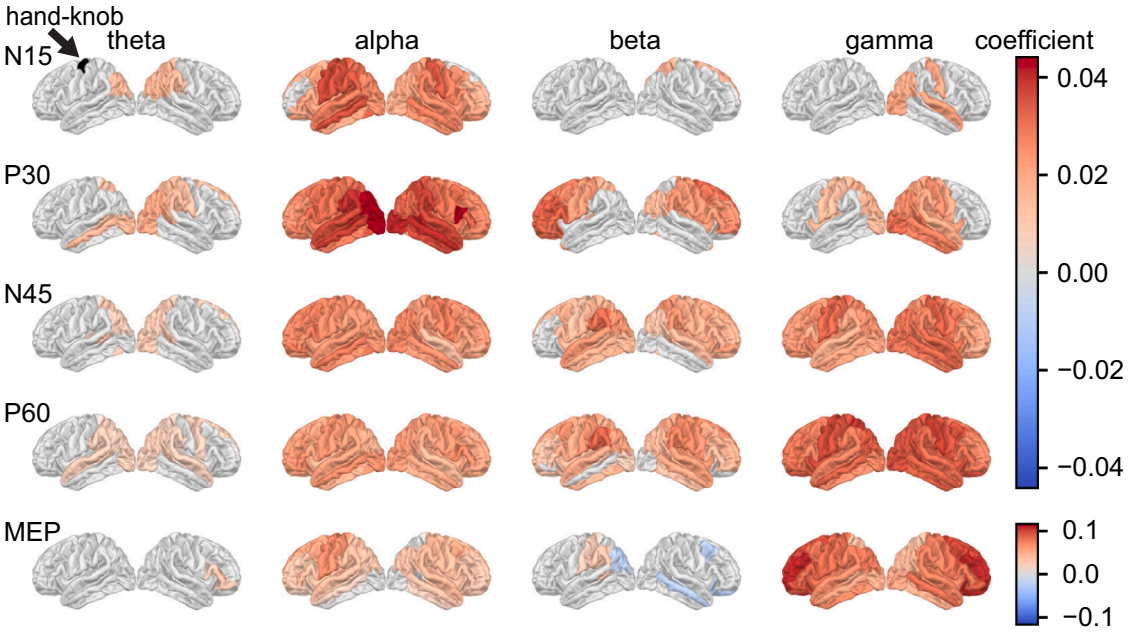

Fig. 2. Band-power coefficients of linear mixed-effects models. Each anatomical parcel represents the frequency band-power coefficient of the model of the respective parcel modeling the respective response. Gray regions indicate insignificant ($p \geq 0.05$; Bonferroni corrected) coefficients. The predictors were scaled to zero mean and unit variance. The frequency ranges were derived based on individual alpha peaks (9.7 ± 1.2 Hz), resulting in average ranges of theta = 3.8–7.3, alpha = 7.3–12.3, beta = 12.3–32.3, and gamma = 32.3–82.3 Hz (see Section 4 in the Supplementary Material for more information). Note that the colorbar scale is different for TEPs and MEPs. The motor hand-knob parcel is indicated as the black region in the left uppermost brain. Across anatomical parcels, maximum model conditional and marginal R^2 (in %), were, respectively, N15: 70.5 and 0.5, P30: 50.3 and 0.6, N45: 51.2 and 0.6, P60: 34.7 and 1.2, and MEP: 42.8 and 2.1. Note that the number of subjects differs for each response type, which makes the results less comparable. Supposing that other variables are held constant, a coefficient of β implies that a 1 SD change in the log-transformed predictor has an $exp(\beta)$ effect on the non-logged outcome variable, *e.g.*, $exp(0.1) - 1 \approx 10.5\%$.

We observed particularly high across-trial variability in dipole (source-localized TEP) amplitudes and goodness-of-fits (R^2 values). The key characteristics across trials are displayed in Table 1 and Fig. 3. Analysis of the relationship across TEPs and MEPs revealed significant positive correlations across all responses except for N15 (Fig. 3). Notably, TEP–TEP correlations were stronger between temporally adjacent responses compared to TEP–MEP correlations. The amplitudes across trials were always positively correlated with the goodness-of-fit (Fig. 3) with an across-subject standard deviation of 0.14 for N15 and under 0.1 for the subsequent TEPs.

4. Discussion

4.1. Principal advances

The present work introduces a single-trial, source-level extraction method for TMS-evoked potentials and demonstrates that moment-to-moment fluctuations in pre-stimulus EEG band-powers predict both cortical (TEP) and corticospinal (MEP) response amplitudes. By extracting single-trial TEPs from their dominant dipolar sources and modeling amplitudes with linear mixed-effects, we show that high-excitability states of the motor cortex are signaled by elevated sensorimotor alpha, beta, and gamma power, whereas low-excitability states appear when these rhythms are weak. These findings establish a mechanistic link between ongoing oscillations and TMS responsiveness, offering a quantitative foundation for real-time, brain-state-dependent neuromodulation (Bergmann 2018; Humaidan et al. 2024).

4.2. Oscillatory markers of excitability

Sensorimotor μ-alpha rhythm. We observed that greater alpha power in the left sensorimotor cortex and other brain regions predicted larger TEPs and MEPs. Although alpha-frequency activity is often interpreted as an inhibitory “idling” rhythm, a recent real-time EEG-triggered TMS study has shown facilitation of corticospinal output during high-power or alpha states (Bergmann et al. 2019). One explanation is that synchronous alpha activity represents a low-noise "readiness" state in which neurons require less additional input to reach firing threshold. This view also fits with cognitive work linking alpha to efficient information gating during memory encoding and retrieval (Klimesch 1999).

Beta and gamma rhythms. Increases in beta and gamma power were positive predictors for later-latency TEP amplitudes, whereas prefrontal gamma power uniquely predicted MEP size. These rhythms are closely coupled to local excitation–inhibition balance; fast beta and gamma oscillations in the motor cortex scale with intracortical GABAergic inhibition and learning capacity (Rossiter et al. 2014; Rempe et al. 2022; Zich et al. 2025). Elevated beta and gamma activity may also mark a predictive or preparatory network state in which pyramidal neurons are synchronously primed for external perturbation — consistent with the idea that participants implicitly anticipate both the TMS click and the ensuing finger twitch.

Network-level influences. Beyond the stimulated primary motor cortex, we identified frontal gamma sources that modulated MEP amplitudes, suggesting that distributed sensorimotor and premotor circuits shape local excitability. This aligns with evidence that large-scale oscillatory networks predict corticospinal output (Ermolova et al. 2024; Haxel et al. 2025). Together, the data support a model in which instantaneous excitability is determined not only by local oscillations but also by the broader functional network state.

4.3. Technical confounds: coil control and hotspot fidelity

Coil deviations exerted a markedly greater influence on MEPs than on TEPs, because even small spatial errors shift the induced current away from the optimal corticospinal hotspot, whereas a distributed

Table 1
Response characteristics across MEPs and TEP components fitted to single trials. Values are presented as mean ± standard deviation (STD). Parameters with "mean" and "STD" are within-subject means and STDs. N: Number of included subjects whose dipole fitted to the average response had an R^2 of at least 75 % and an amplitude of at least 20 nAm (not the average dipole fit across trials, which is displayed in the Table). Amplitude: Absolute value of dipole strength (non-scalar amplitude). Dipole PTP (peak-to-peak): Sensor-space PTP of the forward-projected dipole. PTP data: Sensor-space PTP at the time of the dipole (or the MEP PTP) and ΔPTP is the PTP difference between the forward predicted dipole and sensor-space PTP. The PTPs are calculated as min-max differences. Latency: Post-stimulus latency of the optimal dipole fit. Window size: Width of the fitting time range. See Table 3 in the Supplementary Materials for average responses.

Parameter	N15	P30	N45	P60	MEP
Fit Overview, *N*=	11	23	41	45	50
R^2 mean (%)	61.5 ± 14.5	44.9 ± 14.9	49.6 ± 12.8	55.5 ± 13.9	-
R^2 STD (%)	19.1 ± 4.4	22.1 ± 2.8	22.9 ± 2.3	21.9 ± 3.1	-
Amplitude mean (nAm)	124.3 ± 140.5	87.0 ± 73.5	129.4 ± 95.3	106.0 ± 46.2	-
Amplitude STD (nAm)	58.0 ± 76.3	47.3 ± 36.5	63.8 ± 44.7	49.3 ± 25.9	-
Dipole PTP mean (μV)	16.0 ± 6.8	13.9 ± 8.6	18.9 ± 7.7	19.0 ± 5.8	-
Dipole PTP STD (μV)	7.0 ± 2.4	7.4 ± 3.8	9.3 ± 3.8	8.7 ± 2.6	-
PTP data mean (μV)	21.6 ± 8.4	22.5 ± 10.3	29.5 ± 9.7	28.8 ± 7.8	1144 ± 1030
PTP data STD (μV)	7.4 ± 2.8	8.5 ± 3.4	10.4 ± 3.6	10.1 ± 3.1	906 ± 641
ΔPTP mean (μV)	5.7 ± 3.5	8.7 ± 4.2	10.7 ± 4.2	9.9 ± 4.0	-
ΔPTP STD (μV)	4.2 ± 2.2	6.2 ± 2.8	7.5 ± 2.8	6.7 ± 2.5	-
Latency mean (ms)	16.7 ± 1.9	32.8 ± 3.5	47.4 ± 2.2	62.8 ± 3.5	-
Latency STD (ms)	2.4 ± 0.5	1.7 ± 0.6	2.5 ± 0.7	4.0 ± 1.2	-
Window size (ms)	7.7 ± 1.4	5.1 ± 1.7	7.5 ± 2.3	12.2 ± 4.0	30.0

cortical response can still be evoked at nearby sites. Furthermore, is likely that the effect of coil deviations is larger in reality as the mapped hotspot and the deviations from the mapped hotspot can result in higher or lower effective stimulation of the true hotspot, resulting in higher or lower MEP (or TEP) amplitudes, respectively. The effect of coil control and hotspot fidelity could both be addressed by robotic control and machine learning-based MEP or TEP hotspot mapping (Matsuda et al. 2024; Nieminen et al. 2022; Tervo et al. 2022).

4.4. *Methodological strengths and limitations*

Our single-trial pipeline leveraged spatiotemporal priors from the grand-average TEP to constrain dipole location and orientation, thereby reducing the danger of overfitting to the low-SNR post-pulse interval and to ongoing oscillations. The approach yielded (*i*) significant scalar amplitude TEP–TEP correlations across contiguous trials, (*ii*) systematic relationships between pre-stimulus power and response amplitude, and (*iii*) spatially focal predictors that peaked at the stimulation and response sites — all hallmarks of genuine physiological signal rather than noise. However, response overlap and non-causal artifact correction methods within the post-stimulus-focused periods can cause inconsistencies in TEP–TEP correlations and in coefficient similarity in the LMMs.

Alternative strategies — *e.g.*, sensor-level peak-to-peak measures, fitting free-orientation dipoles, or expanding to multi-source models — can improve numerical goodness-of-fit but risk "chasing" noise or volume-conducted ongoing oscillations. We therefore prioritized specificity over raw fitting accuracy in exchange for cleaner neuroanatomical interpretability. However, while fixing the dipole orientation to the dominant orientation suppresses the contribution of other sources, it also limits the effects of true TEP orientation variability at the location of interest. A pragmatic future compromise could involve pooling early TEP features across two or three consecutive trials to boost SNR without sacrificing temporal resolution.

Residual TMS-related artifacts remain an inevitable concern. Despite the use of SOUND (Mutanen et al. 2018) and SSP–SIR (Mutanen et al. 2016), these artifacts may still contaminate early TEPs, which likely show up as increased early amplitudes and decreased spatiotemporal fidelity in source localization (see Table 3 and Fig. 2 in the Supplementary Materials). Additionally, trials with high-frequency power pre and post TMS can also indicate the increased presence of artifacts and noise. This could lead to non-plausible dipoles with high-amplitudes, possibly distorting the effect between high-power modulations and response amplitude. We therefore advise combining subject-specific stimulation sites that elicit high-SNR TEPs (Casarotto et al. 2022; Mutanen et al. 2013) with adaptive, per-subject preprocessing parameters in future work.

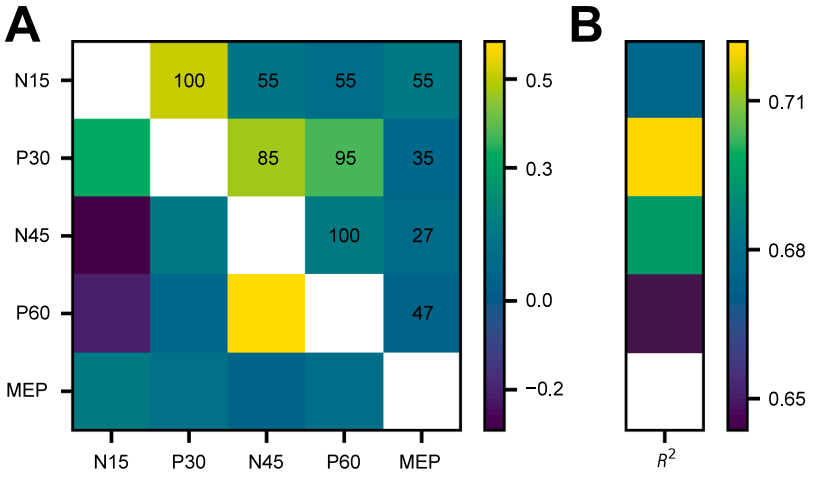

Fig. 3. Spearman correlation analysis of response amplitudes. A: The lower triangle shows the mean, and the upper triangle shows the standard deviation, of significant ($p<0.05$) correlation coefficients of response amplitudes across trials. TEP–TEP correlations are calculated with scalar amplitudes and TEP–MEP correlations with absolute amplitudes. The percentage of subjects with significant correlations is displayed in the respective cell. **B**: Mean correlations between absolute TEP (dipole) amplitudes and dipole R^2 (always significant; $p<0.05$). Only subjects reported in Table 1 are included in the analysis.

4.5. Toward real-time, brain-state-dependent stimulation

Because the fixed-effects predictors are small and explained only a modest share of variance (marginal $R^2 \approx 1$–2%), closed-loop algorithms that continuously maximize response amplitude — rather than relying on static thresholds — are likely to outperform simple EEG biomarkers. Our source-level TEP read-out offers a feedback channel reflecting cortical excitability and is not confounded by spinal factors that affect MEPs. A possible pipeline would be

1. **Calibration:** Collect 100 open-loop trials to fit individualized ICA, SOUND, and SSP–SIR filters, acquire dipolar TEP estimates, and oscillatory predictors.
2. **Online tracking:** Monitor alpha, beta, and gamma power at the stimulation site, at its frontal network nodes, and at the site of the TEP.
3. **Adaptive scheduling:** Deliver the next pulse at the predicted peak-excitability window — or postpone it if a low-excitability window is detected.
4. **Continuous re-learning:** Update the filter and model weights every 30 trials to account for slow drifts (time-on-task "trends") and fatigue.

While statistically significant physiologically interpretable weak predictors may provide useful insights, they can also lead to high false positive and negative rates, limiting their suitability for closed-loop applications. Prior to clinical applications, further investigation is needed into the temporal adjacency of feature fluctuations preceding stimulation, their effects on response amplitudes, and the development of continuously adaptive methods. In practice, with the cost of reduced interpretability, adaptive models using unconstrained features may be preferable if they provide sufficient predictive power, especially as apparent significance in weak predictors can be driven merely by high trial counts.

5. Conclusions

Our results suggest that single-trial, source-resolved TEPs can be reliably extracted and that fluctuations in alpha, beta, and gamma frequency power shortly before stimulation are signatures of motor cortical and corticospinal excitability. In practical terms, these findings can contribute for EEG-informed, brain state-dependent TMS as a potential approach to enhance neuromodulatory effects — both within and beyond motor cortex.

Data availability

The main code used in this study is publicly available and can be accessed at https://github.com/OAhola/TEP_MEP_Predictions.

Ethics statement

The study was approved by the ethics committees of the University of Tübingen (810/2021BO2) and the Helsinki University Hospital (HUS/1198/2016). The study was conducted in compliance with the Declaration of Helsinki.

Declaration of generative AI and AI-assisted technologies in the writing process

During the preparation of this work the author(s) used ChatGPT and Gemini in order to make refinements to the text. After using this tool, the author(s) reviewed and edited the content as needed and take(s) full responsibility for the content of the published article.

CRediT authorship contribution statement

Oskari Ahola: Writing – review & editing, Writing – original draft, Visualization, Validation, Software, Methodology, Investigation, Formal analysis, Data curation, Conceptualization. **Lisa Haxel:** Writing – review & editing, Visualization, Software, Conceptualization. **Maria Ermolova:** Writing – review & editing, Investigation, Data curation. **Dania Humaidan:** Writing – review & editing, Investigation. **Tuomas P. Mutanen:** Writing – review & editing, Investigation. **Mikael Laine:** Writing – review & editing, Investigation. **Matilda Makkonen:** Writing – review & editing, Investigation, Data curation. **Elena Ukharova:** Writing – review & editing, Investigation, Data curation. **Timo Roine:** Writing – review & editing, Investigation. **Pantelis Lioumis:** Writing – review & editing, Supervision, Investigation. **Roberto Guidotti:** Writing – review & editing. **Risto J. Ilmoniemi:** Writing – review & editing, Project administration, Funding acquisition. **Ulf Ziemann:** Writing – review & editing, Supervision, Project administration, Funding acquisition, Conceptualization.

Declaration of competing interest

R.J.I is a founder of Cortisys Inc. P.L is a consultant to Nexstim Plc. for TMS–EEG applications and speech cortical mapping. T.P.M is employed by Nexstim Plc.

Acknowledgements

This study has received funding from the European Research Council (ERC) under the European Unizon's Horizon 2020 research and innovation programme (Grant agreement No 810377). We thank Maxim Schaier, Aishwarya Bagal, Athea Laske, Hailin Wang, Olivier Roy, David Vetter, Noora Kainulainen, Ida Granö, Maria Nazarova, Shokoofeh Parvin, Ana Soto, Ida Ilmoniemi, Timo Tommila, and Ilkka Rissanen for assistance in TMS–EEG measurements, Joonas Laurinoja for measurements assistance and protocol structuring in Aalto, and Miriam Kirchhoff and David Vetter for discussions on phase-effects. We also thank Pedro Gordon and Andreas Jooß for assistance in MRI data collection. We additionally thank Prof. Gian Luca Romani, Prof. Laura Marzetti, Prof. Vittorio Pizzella, Delia Lucarelli, and Giulia Pieramico for feedback on the text.

Supplementary materials

Supplementary material associated with this article can be found, in the online version, at doi:10.1016/j.neuroimage.2025.121553.

References

Bembenek, Jan P., Kurczych, Katarzyna, Klysz, Bożena, Cudna, Agnieszka, Antczak, Jakub, Członkowska, Anna, 2020. Prediction of recovery and outcome using motor evoked potentials and brain derived neurotrophic factor in subacute stroke. J. Stroke Cerebrovasc. Dis. 29 (11), 105202. https://doi.org/10.1016/j.jstrokecerebrovasdis.2020.105202.

Bergmann, Til O., 2018. Brain State-dependent Brain stimulation. Front. Psychol. 9 (November). https://doi.org/10.3389/fpsyg.2018.02108.

Bergmann, Til O., Lieb, Anne, Zrenner, Christoph, Ziemann, Ulf, 2019. Pulsed facilitation of corticospinal excitability by the sensorimotor μ-alpha rhythm. J. Neurosci. 39 (50), 10034–10043. https://doi.org/10.1523/JNEUROSCI.1730-19.2019.

Casarotto, Silvia, Fecchio, Matteo, Rosanova, Mario, et al., 2022. The Rt-TEP tool: real-time visualization of TMS-evoked potentials to maximize cortical activation and minimize artifacts. J. Neurosci. Methods 370 (March), 109486. https://doi.org/10.1016/j.jneumeth.2022.109486.

Casarotto, Silvia, Lauro, Leonor J.Romero, Bellina, Valentina, et al., 2010. EEG responses to TMS are sensitive to changes in the perturbation parameters and repeatable over time. PloS One 5 (4), e10281. https://doi.org/10.1371/journal.pone.0010281.

Delorme, Arnaud, Makeig, Scott, 2004. EEGLAB: an open source toolbox for analysis of single-trial EEG dynamics including independent component analysis. J. Neurosci. Methods 134 (1), 9–21. https://doi.org/10.1016/j.jneumeth.2003.10.009.

Desikan, Rahul S., Ségonne, Florent, Fischl, Bruce, et al., 2006. An automated labeling system for subdividing the Human cerebral cortex on MRI scans into gyral based

regions of interest. NeuroImage 31 (3), 968–980. https://doi.org/10.1016/j.neuroimage.2006.01.021.
Ermolova, Maria, Metsomaa, Johanna, Belardinelli, Paolo, Zrenner, Christoph, Ziemann, Ulf, 2024. Blindly separated spontaneous network-level oscillations predict corticospinal excitability. J. Neural Eng. 21 (3). https://doi.org/10.1088/1741-2552/ad5404.
Gosseries, Olivia, Sarasso, Simone, Casarotto, Silvia, et al., 2015. On the cerebral origin of EEG responses to TMS: insights from severe cortical lesions. Brain Stimul. 8 (1), 142–149. https://doi.org/10.1016/j.brs.2014.10.008.
Gramfort, Alexandre, Luessi, Martin, Larson, Eric, et al., 2013. MEG and EEG data analysis with MNE-python. Front. Neurosci. 7 (December). https://doi.org/10.3389/fnins.2013.00267.
Groth, Christopher L., Singh, Arun, Zhang, Qiang, Berman, Brian D., Narayanan, Nandakumar S., 2021. GABAergic modulation in movement related oscillatory activity: a review of the effect pharmacologically and with aging. Tremor Other Hyperkinetic Mov. 11 (1). https://doi.org/10.5334/tohm.655.
Hallett, Mark., 2007. Transcranial magnetic stimulation: a primer. Neuron 55 (2), 187–199. https://doi.org/10.1016/j.neuron.2007.06.026.
Hämäläinen, Matti S., Ilmoniemi, Risto J., 1994. Interpreting magnetic fields of the brain: minimum norm estimates. Med. Biol. Eng. Comput. 32 (1), 35–42. https://doi.org/10.1007/BF02512476.
Haxel, Lisa, Ahola, Oskari, Belardinelli, Paolo, et al., 2025. Decoding motor excitability in TMS using EEG-features: an exploratory machine learning approach. IEEE Trans. Neural Syst. Rehabil. Eng. 33, 103–112. https://doi.org/10.1109/TNSRE.2024.3516393.
Henderson, C.J., Butler, S.R., Glass, A., 1975. The localization of equivalent dipoles of EEG sources by the application of electrical field theory. Electroencephalogr. Clin. Neurophysiol. 39 (2), 117–130. https://doi.org/10.1016/0013-4694(75)90002-4.
Herrmann, Christoph S., Fründ, Ingo, Lenz, Daniel, 2010. Human gamma-band activity: a review on cognitive and behavioral correlates and network models. Neurosci. Biobehav. Rev. 34 (7), 981–992. https://doi.org/10.1016/j.neubiorev.2009.09.001. Binding processes: Neurodynamics and functional role in memory and action.
Hordacre, Brenton, Ghosh, Rukmini, Goldsworthy, Mitchell R., Ridding, Michael C., 2019. Transcranial magnetic stimulation-EEG biomarkers of poststroke upper-limb motor function. J. Stroke Cerebrovasc. Dis. 28 (12), 104452. https://doi.org/10.1016/j.jstrokecerebrovasdis.2019.104452.
Humaidan, Dania, Xu, Jiahua, Kirchhoff, Miriam, Romani, Gian Luca, Ilmoniemi, Risto J., Ziemann, Ulf, 2024. Towards real-time EEG-TMS modulation of brain State in a closed-loop approach. Clin. Neurophysiol.: Off. J. Int. Fed. Clin. Neurophysiol. 158 (February), 212–217. https://doi.org/10.1016/j.clinph.2023.12.006.
Hyvärinen, Aapo, Oja, Erkki, 2000. Independent component analysis: algorithms and applications. Neural Netw. 13 (4), 411–430. https://doi.org/10.1016/S0893-6080(00)00026-5.
Ilmoniemi, Risto J., Kičić, Dubravko, 2010. Methodology for combined TMS and EEG. Brain Topogr. 22 (4), 233–248. https://doi.org/10.1007/s10548-009-0123-4.
Ilmoniemi, Risto J., Virtanen, Juha, Ruohonen, Jarmo, et al., 1997. Neuronal responses to magnetic stimulation reveal cortical reactivity and connectivity. Neuroreport 8 (16), 3537–3540. https://doi.org/10.1097/00001756-199711100-00024.
Klimesch, Wolfgang., 1999. EEG alpha and theta oscillations reflect cognitive and memory performance: a review and analysis. Brain Res. Rev. 29 (2), 169–195. https://doi.org/10.1016/S0165-0173(98)00056-3.
Klimesch, Wolfgang, Sauseng, Paul, Hanslmayr, Simon, 2007. EEG alpha oscillations: the inhibition–Timing hypothesis. Brain Res. Rev. 53 (1), 63–88. https://doi.org/10.1016/j.brainresrev.2006.06.003.
Lefaucheur, Jean-Pascal, Aleman, André, Baeken, Chris, et al., 2020. Evidence-based guidelines on the therapeutic use of repetitive transcranial magnetic stimulation (rTMS): an update (2014–2018). Clin. Neurophysiol. 131 (2), 474–528. https://doi.org/10.1016/j.clinph.2019.11.002.
Lindstrom, Mary J., Bates, Douglas M., 1988. Newton—Raphson and EM algorithms for linear mixed-effects models for repeated-measures data. J. Am. Stat. Assoc. 83 (404), 1014–1022. https://doi.org/10.1080/01621459.1988.10478693.
Lioumis, Pantelis, Kičić, Dubravko, Savolainen, Petri, Mäkelä, Jyrki P., Kähkönen, Seppo, 2009. Reproducibility of TMS—Evoked EEG responses. Hum. Brain Mapp. 30 (4), 1387–1396. https://doi.org/10.1002/hbm.20608.
Matsuda, Renan H., Souza, Victor H., Marchetti, Thais C., et al., 2024. Robotic–Electronic platform for autonomous and accurate transcranial magnetic stimulation targeting. Brain Stimul. 17 (2), 469–472. https://doi.org/10.1016/j.brs.2024.03.022.
Mutanen, Tuomas P., Biabani, Mana, Sarvas, Jukka, Ilmoniemi, Risto J., Rogasch, Nigel C., 2020. Source-based artifact-rejection techniques available in TESA, an open-Source TMS–EEG toolbox. Brain Stimul. 13 (5), 1349–1351. https://doi.org/10.1016/j.brs.2020.06.079.
Mutanen, Tuomas P., Kukkonen, Matleena, Nieminen, Jaakko O., Stenroos, Matti, Sarvas, Jukka, Ilmoniemi, Risto J., 2016. Recovering TMS-evoked EEG responses masked by muscle artifacts. NeuroImage 139 (October), 157–166. https://doi.org/10.1016/j.neuroimage.2016.05.028.
Mutanen, Tuomas P., Mäki, Hanna, Ilmoniemi, Risto J., 2013. The effect of stimulus parameters on TMS–EEG muscle artifacts. Brain Stimul. 6 (3), 371–376. https://doi.org/10.1016/j.brs.2012.07.005.
Mutanen, Tuomas P., Metsomaa, Johanna, Liljander, Sara, Ilmoniemi, Risto J., 2018. Automatic and robust noise suppression in EEG and MEG: the SOUND algorithm. NeuroImage 166 (February), 135–151. https://doi.org/10.1016/j.neuroimage.2017.10.021.
Nakagawa, Shinichi, Schielzeth, Holger, 2013. A general and simple method for obtaining r^2 from generalized linear mixed-effects models. Methods Ecol. Evol. 4 (2), 133–142. https://doi.org/10.1111/j.2041-210x.2012.00261.x.
Nieminen, Jaakko O., Sinisalo, Heikki, Souza, Victor H., et al., 2022. Multi-locus transcranial magnetic stimulation system for electronically targeted brain stimulation. Brain Stimul. 15 (1), 116–124. https://doi.org/10.1016/j.brs.2021.11.014.
Pellicciari, Maria Concetta, Bonnì, Sonia, Ponzo, Viviana, et al., 2018. Dynamic reorganization of TMS-evoked activity in subcortical stroke patients. NeuroImage 175 (July), 365–378. https://doi.org/10.1016/j.neuroimage.2018.04.011.
Pion-Tonachini, Luca, Kreutz-Delgado, Ken, Makeig, Scott, 2019. ICLabel: an automated electroencephalographic independent component classifier, dataset, and website. NeuroImage 198 (September), 181–197. https://doi.org/10.1016/j.neuroimage.2019.05.026.
Rempe, Maggie P., Lew, Brandon J., Embury, Christine M., Christopher-Hayes, Nicholas J., Schantell, Mikki, Wilson, Tony W., 2022. Spontaneous sensorimotor beta power and cortical thickness uniquely predict motor function in healthy aging. NeuroImage 263 (November), 119651. https://doi.org/10.1016/j.neuroimage.2022.119651.
Rogasch, Nigel C., Sullivan, Caley, Thomson, Richard H., et al., 2017. Analysing concurrent transcranial magnetic stimulation and electroencephalographic data: a review and introduction to the open-source TESA software. NeuroImage 147 (February), 934–951. https://doi.org/10.1016/j.neuroimage.2016.10.031.
Rossini, P.M., Burke, D., Chen, R., et al., 2015. Non-invasive electrical and magnetic stimulation of the brain, spinal cord, roots and peripheral nerves: basic principles and procedures for routine clinical and research application. An updated report from an I.F.C.N. Committee. Clin. Neurophysiol.: Off. J. Int. Fed. Clin. Neurophysiol. 126 (6), 1071–1107. https://doi.org/10.1016/j.clinph.2015.02.001.
Rossiter, Holly E., Davis, Emma M., Clark, Ella V., Boudrias, Marie-Hélène, Ward, Nick S., 2014. Beta oscillations reflect changes in motor cortex inhibition in healthy ageing. Neuroimage 91 (100), 360–365. https://doi.org/10.1016/j.neuroimage.2014.01.012.
Russo, S., Sarasso, S., Puglisi, G.E., et al., 2022. TAAC - TMS adaptable auditory control: a universal tool to mask TMS clicks. J. Neurosci. Methods 370 (March), 109491. https://doi.org/10.1016/j.jneumeth.2022.109491.
Sarvas, Jukka., 1987. Basic mathematical and electromagnetic concepts of the biomagnetic inverse problem. Phys. Med. Biol. 32 (1), 11–22. https://doi.org/10.1088/0031-9155/32/1/004.
Seabold, Skipper, Perktold, Josef, 2010. Statsmodels: econometric and statistical modeling with python. Scipy. https://doi.org/10.25080/Majora-92bf1922-011 ahead of print, May.
Strafella, Rebecca, Momi, Davide, Zomorrodi, Reza, et al., 2023. Identifying neurophysiological markers of intermittent theta burst stimulation in treatment-resistant depression using transcranial magnetic stimulation–Electroencephalography. Biol. Psychiatry Neural Codes Depress. Treat. 94 (6), 454–465. https://doi.org/10.1016/j.biopsych.2023.04.011.
Tervo, Aino E., Nieminen, Jaakko O., Lioumis, Pantelis, et al., 2022. Closed-loop optimization of transcranial magnetic stimulation with electroencephalography feedback. Brain Stimul. 15 (2), 523–531. https://doi.org/10.1016/j.brs.2022.01.016.
Thies, Miriam, Zrenner, Christoph, Ziemann, Ulf, Bergmann, Til O., 2018. Sensorimotor mu-alpha power is positively related to corticospinal excitability. Brain Stimul. 11 (5), 1119–1122. https://doi.org/10.1016/j.brs.2018.06.006.
Virtanen, Pauli, Gommers, Ralf, Oliphant, Travis E., et al., 2020. SciPy 1.0: fundamental algorithms for scientific computing in Python. Nat. Methods 17 (3), 261–272. https://doi.org/10.1038/s41592-019-0686-2.
Voineskos, Daphne, Blumberger, Daniel M., Zomorrodi, Reza, et al., 2019. Altered transcranial magnetic stimulation-electroencephalographic markers of inhibition and excitation in the dorsolateral prefrontal cortex in major depressive disorder. Biol. Psychiatry 85 (6), 477–486. https://doi.org/10.1016/j.biopsych.2018.09.032.
Vucic, Steve, Stanley Chen, Kai-Hsiang, Kiernan, Matthew C., et al., 2023. Clinical diagnostic utility of transcranial Magnetic stimulation in neurological disorders. Updated report of an IFCN committee. Clin. Neurophysiol.: Off. J. Int. Fed. Clin. Neurophysiol. 150 (June), 131–175. https://doi.org/10.1016/j.clinph.2023.03.010.
Wischnewski, Miles, Haigh, Zachary J., Shirinpour, Sina, Alekseichuk, Ivan, Opitz, Alexander, 2022. The phase of sensorimotor mu and beta oscillations has the opposite effect on corticospinal excitability. Brain Stimul. 15 (5), 1093–1100. https://doi.org/10.1016/j.brs.2022.08.005.
Zich, Catharina, Nowak, Magdalena, Hinson, Emily L., et al., 2025. Human motor cortical gamma activity relates to GABAergic intracortical inhibition and motor learning. Imaging Neurosci. 3 (April). https://doi.org/10.1162/imag_a_00538 imag_a_00538.
Zrenner, Christoph, Desideri, Debora, Belardinelli, Paolo, Ziemann, Ulf, 2018. Real-time EEG-defined excitability states determine efficacy of TMS-induced plasticity in Human motor cortex. Brain Stimul. 11 (2), 374–389. https://doi.org/10.1016/j.brs.2017.11.016.